

Article

# Areal-Averaged Spectral Surface Albedo in an Atlantic Coastal Area: Estimation from Ground-Based Transmission

Evgueni Kassianov <sup>1,\*</sup>, James Barnard <sup>2</sup>, Connor Flynn <sup>1</sup>, Laura Riihimaki <sup>1</sup> , Larry K. Berg <sup>1</sup> and David A. Rutan <sup>3</sup>

<sup>1</sup> Atmospheric Sciences & Global Change Division, Pacific Northwest National Laboratory, Richland, WA 99352, USA; Connor.Flynn@pnnl.gov (C.F.); Laura.Riihimaki@pnnl.gov (L.R.); Larry.Berg@pnnl.gov (L.K.B.)

<sup>2</sup> Department of Physics, University of Nevada, Reno, NV 89557, USA; jbarnard@unr.edu

<sup>3</sup> Science Systems and Applications, Inc., Hampton, VA 23666, USA; David.A.Rutan@NASA.gov

\* Correspondence: Evgueni.Kassianov@pnnl.gov; Tel.: +1-509-372-6535

Received: 10 April 2017; Accepted: 29 June 2017; Published: 12 July 2017

**Abstract:** Tower-based data combined with high-resolution satellite products have been used to produce surface albedo at various spatial scales over land. Because tower-based albedo data are available at only a few sites, surface albedos using these combined data are spatially limited. Moreover, tower-based albedo data are not representative of highly heterogeneous regions. To produce areal-averaged and spectrally-resolved surface albedo for regions with various degrees of surface heterogeneity, we have developed a transmission-based retrieval and demonstrated its feasibility for relatively homogeneous land surfaces. Here, we demonstrate its feasibility for a highly heterogeneous coastal region. We use the atmospheric transmission measured during a 19-month period (June 2009–December 2010) by a ground-based Multi-Filter Rotating Shadowband Radiometer (MFRSR) at five wavelengths (0.415, 0.5, 0.615, 0.673 and 0.87  $\mu\text{m}$ ) at the Department of Energy’s Atmospheric Radiation Measurement (ARM) Mobile Facility (AMF) site located on Graciosa Island. We compare the MFRSR-retrieved areal-averaged surface albedo with albedo derived from Moderate Resolution Imaging Spectroradiometer (MODIS) observations, and also a composite-based albedo. We demonstrate that these three methods produce similar spectral signatures of surface albedo; however, the MFRSR-retrieved albedo, is higher on average ( $\leq 0.04$ ) than the MODIS-based areal-averaged surface albedo and the largest difference occurs in winter.

**Keywords:** Multi-Filter Rotating Shadowband Radiometer (MFRSR); Moderate Resolution Imaging Spectroradiometer (MODIS) observations; atmospheric transmission; areal-averaged surface albedo; spectral and seasonal variability; Atmospheric Radiation Measurement (ARM) Program Mobile Facility (AMF); coastal region; Graciosa Island; Azores

## 1. Introduction

Knowing that surface albedo substantially affects the variability of the Earth’s radiation balance [1], and that this variability is sensitive to multiple natural and man-made factors [2], the importance of monitoring the surface albedo from ground, air and space [3–7] is increasingly recognized. The assessment of these variations is challenging for heterogeneous regions where complex landscapes with distinctive land cover types occur. Conventionally, the required assessment is based on the synergistic use of “point” tower-based measurements of surface albedo together with satellite images, such as Landsat Enhanced Thematic Mapper Plus (EMT+) imagery [4,5]. The combination of ground- and satellite-based data offers a capability to derive the high spatial resolution ( $\sim 0.1$  km) albedo

product and, consequently the corresponding coarse-resolution product at a given spatial scale using existing upscaling procedures. Since tower-based albedo data are available at only a few long-term sites [6,7], application of this conventional approach is quite limited. Moreover, obtaining the combined tower-based data and high-resolution satellite product and their subsequent upscaling make this approach rather difficult and time-consuming. In this context, development of complementary tools for obtaining the coarse spatial resolution (~1–10 km) albedo product is highly desirable.

Recently, we have developed a simple retrieval of the areal-averaged and spectrally-resolved surface albedo [8] to address the above mentioned issues associated with complex heterogeneous landscapes. Our approach involves atmospheric transmission measured by a ground-based upward facing Multi-Filter Rotating Shadowband Radiometer (MFRSR) at five wavelengths (0.415, 0.5, 0.615, 0.675, and 0.87  $\mu\text{m}$ ) under fully overcast conditions. Compared to the tower-based data, MFRSR measurements are abundant and represent both short- and long-term deployments in the climate-important regions around the world [9,10]. Also, we have demonstrated good agreement between the spectrally-resolved values of surface albedo retrieved by our MFRSR-based approach and those measured by towers and derived from Moderate Resolution Imaging Spectroradiometer (MODIS) observations for relatively homogeneous surfaces in the Southern Great Plains of North America [8]. Here, we illustrate the performance of our retrieval for a coastal region with a highly heterogeneous surface (including land and ocean) and compare the MFRSR-retrieved values of the areal-averaged albedo with those obtained by two conventional approaches based on high resolution satellite images and MODIS data. The main objective of our comparison is to illustrate the level of agreement between the areal-averaged albedos provided by three methods under these challenging observational conditions rather than documenting the superiority of one of these three methods.

## 2. Observations

We apply MFRSR data collected at the U.S. Department of Energy's (DOE's) Atmospheric Radiation Measurement (ARM) Program Mobile Facility (AMF; [11]). The AMF was located at the northern end of Graciosa Island, Azores (39.09° N, 28.03° W) in the eastern Atlantic Ocean. The AMF deployment [12] was designed to acquire both quantitative and qualitative information about the temporal variability of cloud, aerosol and radiative properties and, thus provide the impetus and observational basis to better understand the complex processes occurring in climatically important coastal areas [13,14]. In particular, these processes are responsible for frequent and optically thick clouds as illustrated by annual mean values of the total cloud fraction and total cloud optical depth, which are about 0.7 and 13, respectively [13]. Compared to middle (3–6 km) and high (>6 km) clouds, single-layered low (<3 km) clouds are more prominent at the AMF site and are located quite close to the surface with an annual mean cloud base height (CBH) of approximately 1 km [13]. It should be noted that satellite-based retrievals of the surface albedo require clear-sky conditions (Section 3). Therefore, the frequent cloudy days observed at the AMF site pose challenges for these retrievals and lead to relatively few measurements. In contrast, the cloudy days represent favorable conditions for our ground-based retrievals since it uses an overcast cloud layer as a "mirror" to retrieve the areal-averaged surface albedo (Section 3). Our retrieval utilizes the atmospheric transmission measured at five wavelengths (0.415, 0.5, 0.615, 0.675, and 0.87  $\mu\text{m}$ ) by the MFRSR, which is part of the AMF instrumentation suite.

An area with moderate size (~2 × 2 km<sup>2</sup>) surrounding the AMF site includes regions with soil, vegetation and ocean (Figure 1). These three types of surface have distinct visual appearances: "brown" (soil), "green" (vegetation) and "navy and white" ocean associated with the open ocean, whitecaps at high wind speed and breaking waves near shore. Similar differences occur with regard to the type-dependent surface albedo [15–17]. The observed surface heterogeneity at the coastal AMF site is much higher than those typical at the continental sites with available tower-based measurements [8,16]. Thus, the observed surface heterogeneity is too complicated for an accurate assessment of the areal-averaged albedo from tower-based measurements. Commonly, tower-based

downward-looking instruments are mounted at several meters above the ground limiting their “site” to a relatively small surface area. For example, if a downward-looking instrument is mounted at 10 m above the surface, more than 90% of the upwelling radiation comes from an area only 60 meters in diameter below the instrument [8]. Such “point” measurements of surface albedo are not representative of an area of interest surrounding the AMF site.

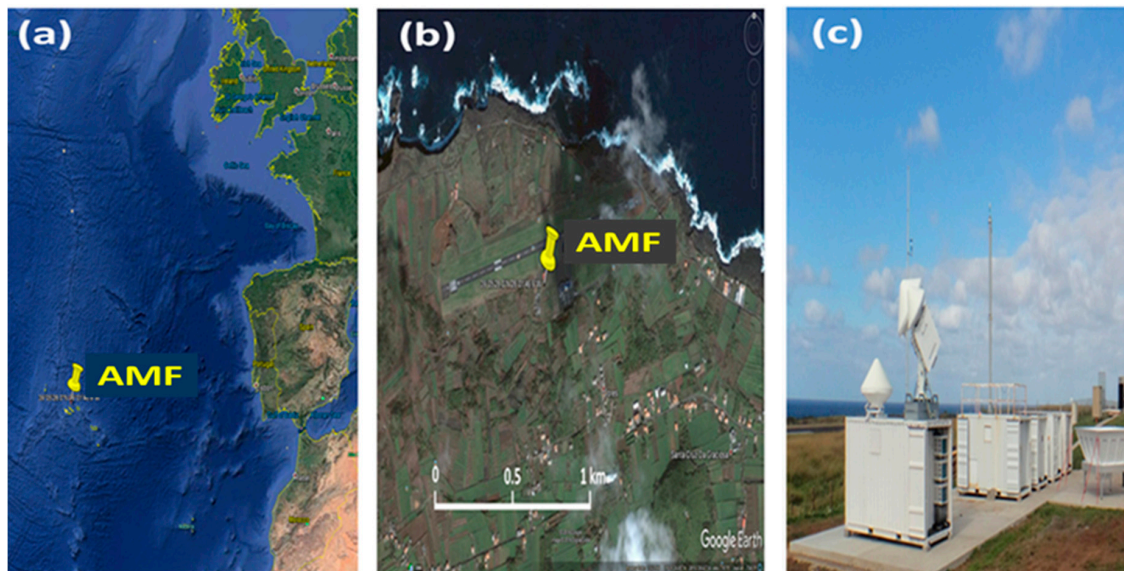


**Figure 1.** Aerial (a,b) and surface (c) images of the Atmospheric Radiation Measurement (ARM) Program Mobile Facility (AMF) site. The aerial and surface images are taken from Google Earth and website [18], respectively. These two images indicate the locations of the ground-based instrumentation suite, which includes the Multi-Filter Rotating Shadowband Radiometer (MFRSR). The suite is surrounded by several sub-areas with different surface types, such as “brown” soil, “green” vegetation and “navy” ocean with whitecaps.

### 3. Approach

In this section, we outline three methods to estimate the areal-averaged albedo and provide the necessary background to section 4 where the corresponding values of surface albedo are compared. We also summarize the main assumptions involved in these three methods and the expected uncertainties of the estimated albedos.

#### 3.1. MFRSR-Based Retrieval

For ground-based MFRSR measurements under fully overcast conditions, the key variable is atmospheric (diffuse) transmission at five wavelengths (0.415, 0.5, 0.615, 0.675, and 0.87  $\mu\text{m}$ ). The measured atmospheric transmission includes sunlight reflected by the ground and then “bounced” back to the surface by the cloud deck. Compared to the cloud optical properties, the surface albedo typically exhibits a strong spectral dependence in the visible and near-infrared spectral range. As a result, the spectral changes of the measured transmission are mainly governed by the surface albedo for a given area of interest. For example, the surface albedo is quite small (less than 0.07) at 0.415  $\mu\text{m}$  wavelength for the majority of land use/land cover types. As a result, the measured transmission at 0.415  $\mu\text{m}$  wavelength represents conditions with a “black” surface where the relative contribution of the surface reflectance to the downward radiation is small. In contrast, the surface albedo for the same surface can be large (up to 0.5) at 0.87  $\mu\text{m}$  wavelength [10,16]. Thus, the measured transmission at 0.87  $\mu\text{m}$  wavelength represents conditions with a relatively “bright” surface where the relative contribution of the surface reflected radiation to the measured downwelling radiation is large.

The spectrally resolved information on surface albedo is obtained by combining the MFRSR-measured transmission at several wavelengths with different relative contributions of the surface albedo. In particular, our simple retrieval under overcast conditions is based on a one-line semi-analytical equation and involves two major steps. For the first step, the cloud optical depth is estimated from the measured transmission at 0.415  $\mu\text{m}$  wavelength using an assumed surface albedo (0.04) and asymmetry factor (0.87) for liquid water clouds. For the second step, the spectral surface albedo at the other MFRSR wavelengths (0.5, 0.615, 0.675, and 0.87  $\mu\text{m}$ ) is estimated using the corresponding spectral values of the measured transmittance, the retrieved cloud optical depth, and assumed asymmetry parameter. It should be emphasized that the transmission-based retrieval defines the areal-averaged values of surface albedo given that the “bounced” sunlight comes to the cloud deck from a wide surface area. This area could be “seen” by a downward-looking airborne radiometer at an altitude equal to the CBH. The size of the “seen” area is proportional to CBH: its radius is approximated roughly as  $R \sim 3\text{CBH}$  for Lambertian surfaces [8].

In addition to the assumptions explicitly involved in our two-step retrieval, several additional factors can contribute to uncertainties of the MFRSR-retrieved albedos [8]. These factors include application of one-dimensional radiative transfer theory that does not account for the small-scale changes of cloud optical properties. To reduce their potential impact on our retrieval, we consider only the daily-averaged values of the retrieved surface albedo. In particular, we use instantaneous values of the measured transmittance to retrieve instantaneous values of surface albedo for a day of interest. Daily-averaged surface albedo is then calculated from the retrieved instantaneous values of surface albedo. Since the diurnal variability of the surface albedo is less pronounced for larger solar zenith angles ( $\mu > 0.4$ , where  $\mu$  is the cosine of solar zenith angle), we restrict our calculations of the averaged values to appropriate conditions ( $\mu > 0.4$ ). The impact of atmospheric aerosol located beneath a cloud layer on the retrievals is neglected and such approximation is reasonable for low-to-moderate aerosol loading (aerosol optical depth  $< 0.4$ ). The expected total uncertainty of the MFRSR-retrieved albedo ( $A_{\lambda}^r$ ) is about 0.03 [8].

### 3.2. Composite-Based Output

Land cover classification can be obtained from high-resolution satellite images [7], thermal remote sensing [19] or land surface models (LSM; [20]). This classification of surface types together with the associated albedos [21] are commonly applied to estimate spectrally-resolved areal-averaged albedo ( $A_{\lambda}^a$ ) using a weighted average approach [16,22]

$$A_{\lambda}^a = \sum_i w_i A_{\lambda,i} \quad (1)$$

where  $w$  and  $A$  represent the weight and surface albedo of the major surface types for a given area (subscript  $i$ ) and wavelength (subscript  $\lambda$ ). The underlying assumption of this approach is that the relative contribution of each surface type to the areal-averaged albedo is proportional to its area fraction and this contribution does not depend on wavelength.

Similar to Cescatti et al. [7], we use a high-resolution satellite image (from Google Earth) for the land cover classification (Figure 1). Visual inspection of the aerial images (Figure 1) at moderate spatial scales ( $\sim 2$  km in diameter) suggests that there are three major surface types at the AMF site and surrounding area: vegetation (grassland), soil and ocean. The corresponding estimated fractions within the area of interest (circle, Figure 2) are: 0.35 (vegetation), 0.25 (soil) and 0.4 (ocean with whitecaps). The associated values of the spectrally resolved surface albedo are available for different surface types from previous studies [15–17,23,24]. We use parameterizations of ocean [15], vegetation [23] and soil [16] surface albedo to approximate the albedo values for three major surface types observed near the AMF site (Table 1). From equation 1, we calculate the areal-averaged albedo using the estimated fractions for three major surface types, and values of spectrally-resolved albedo. Hereinafter, the calculated areal-averaged albedo is referred to as the “composite-based” albedo.

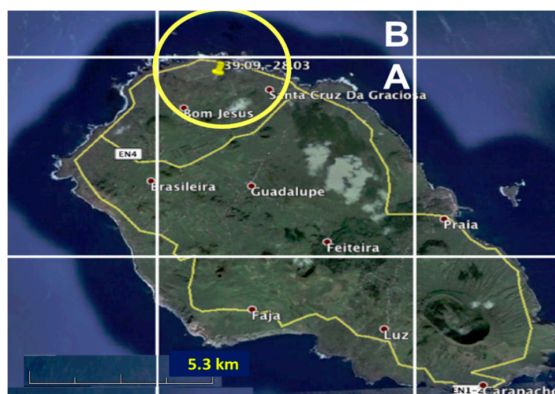


**Figure 2.** An image from Google Earth shows the approximate position of 0.05° grid boxes. The AMF site is located at the northern end of box A. This box represents mostly land and also a small fraction of ocean. The adjacent box B (in the northern direction) characterizes ocean only. A circle (yellow) with radius about 2 km defines an approximate area that is representative of the areal-averaged surface albedo retrieved from MFRSR data.

**Table 1.** Spectrally-resolved values of the surface albedo for vegetation, soil, ocean at five MFRSR wavelengths. It is assumed that that these values are season-independent.

Wavelength (μm)	Vegetation	Soil	Ocean
0.415	0.064	0.040	0.07
0.5	0.115	0.050	0.06
0.615	0.080	0.096	0.051
0.673	0.169	0.118	0.048
0.87	0.531	0.146	0.046

The uncertainties of the composite-based albedo are primarily from the accuracy of the estimated fractions of the major surface types and uncertainties of the associated albedos. For example, “ocean” albedo depends on wind speed (calm versus windy conditions; [15]) and water depth (shallow versus deep waters; [25]), while “soil” albedo is a function of soil type and water content [26]. It should be noted that the impact of foam (Figure 1; whitecaps) on the ocean surface albedo is not captured by the popular parameterizations [15] and whitecap coverage typically increases with wind speed [27]. Given the coastal location of this analysis, whitecaps and breaking waves near shore could have an appreciable impact on the albedo. Moreover, effective reflectance of foam in the visible spectral range is high (from 0.4 to 0.6) [28]. Since we do not know the exact proportions of the surface types (including fractional coverage of highly-reflective foam), nor do we know how well previously reported albedos for different areas represent the surfaces considered here, the expected uncertainties for this method are quite large. We assume that these uncertainties are 30%. Therefore, we take these results more as a qualitative guide to the spectral variation of surface albedo, rather than strictly quantitative values.

### 3.3. MODIS-Derived Albedo

The MODIS product MCD43C2 v005 [29] is used to compute areal-averaged albedo ( $A_{\lambda}^m$ ). MCD43C2 is a gridded product with 0.05° equal angle spatial resolution and described in detail by Gao et al. [30]. This resolution corresponds to an approximate 5 km “box” size (Figure 2). Temporally, this product delivers empirical Bidirectional Reflectance Distribution Functions (BRDFs) from clear sky MODIS imager data every eight days using overlapping 16-day windows [31]. Coefficients are derived from the MODIS visible channels modeling the isotropic, volume, and geometric-optical surface scattering for direct (“Black Sky”) and wholly diffuse (“White Sky”) radiation. The MODIS-based white-sky albedos used here are derived directly from the coefficients supplied on the MCD43C2 data

product using a look-up-table that is a function of aerosol optical depth and aerosol type. Spectrally, the product supplies seven narrowband visible and near infrared channels and three broadband estimates based on weighting functions described by Liang et al. [32]. The accuracy of the MODIS operational albedos marked as high quality by the quality assurance flags is less than 5% relative at validation sites studied thus far and even those albedo values with low quality flags have been found to be within 10% relative of field data [33].

Similar to the composite-based surface albedo, we assume that within the area of interest (circle; Figure 2) the land and ocean fractions are 0.6 and 0.4, respectively. In contrast to the composite-based surface albedo, we define the surface albedo of land from MODIS data. First, we estimate a fraction of land within box A (Figure 2). From visual inspection, we assess area fractions of land ( $w_{land}^A$ ) and ocean ( $w_{ocean}^A$ ) as 0.85 (land) and 0.15 (ocean). Second, we approximate land albedo ( $A_{\lambda,land}^A$ ). To do that, we also assume that the values of ocean albedo for box A ( $A_{\lambda,ocean}^A$ ) and the adjacent box B ( $A_{\lambda,land}^B$ ) are the same. Recall that box B is completely covered by ocean (Figure 2). Using the assessed fractions of land and ocean and the assumed ocean albedo, we calculate the land albedo as

$$A_{\lambda,land}^A = \left( A_{\lambda}^A - w_{ocean}^A A_{\lambda,ocean}^B \right) / w_{land}^A \quad (2)$$

where  $A_{\lambda}^A$  represents the MODIS-derived albedo for box A with land and water areas (Figure 2).

We calculate the areal-averaged surface albedo ( $A_{\lambda}^m$ ) using the weighted average approach (Equation 1), the assumed fractions of land (0.6) and ocean (0.4), the approximated land albedo ( $A_{\lambda,land}^A$ ) and the MODIS-derived ocean albedo ( $A_{\lambda,ocean}^B$ ). Hereinafter, the calculated areal-averaged albedo obtained from the MODIS-derived land albedo is referred to as the “MODIS-based” albedo. To compare  $A_{\lambda}^m$  with the MFRSR-retrieved albedo, we linearly interpolate/extrapolate the spectral MODIS surface albedo values to the four MFRSR wavelengths.

The uncertainties of  $A_{\lambda}^m$  are mainly determined by the accuracy of estimated fractions (ocean versus land) and uncertainties of the MODIS-derived albedo over heterogeneous coastal regions. Comprehensive evaluations of the MODIS-derived land albedos over heterogeneous areas have involved high-resolution satellite images [5] and aircraft [34] measurements. For example, the 0.03-km Landsat data have been coupled with surface tower-based measurements and then up-scaled to the coarse MODIS resolution to evaluate the MODIS albedo product (MCD43A [35], 16-day daily, the shortwave blue-sky albedo) over several heterogeneous sites [5]. The evaluation results (up-scaled 0.051-km Landsat-based albedo versus MODIS-derived albedo) have demonstrated the bias and root mean square error (RMSE) are about 0.025 and 0.03, respectively. In comparison with the collocated and coincident airborne measurements, the MODIS-derived albedo tends to underestimate noticeably (typically 0.025 and up to 0.05) those measured from the air in the visible and near-infrared spectral range (400–900 nm) [34]. We assume that the reported uncertainties are representative for complex coastal conditions considered here and the expected uncertainties in the spectrally-resolved areal-averaged surface albedo are about 0.03.

#### 4. Results

To illustrate qualitative similarities and differences between the MODIS-based ( $A_{\lambda}^m$ ) and MFRSR-retrieved ( $A_{\lambda}^r$ ) areal-averaged albedos, we start with their time series (Figure 3). The latter exhibit “near-flat” seasonal patterns (Figure 3) compared to those acquired at the continental sites [8,16]. Since the MODIS albedo product represents a 16-day period, we calculate 16-day averaged values of the MFRSR-retrieved albedo using a moving boxcar average (16 points). The maximum values ( $\sim 0.25$ ) of the coastal surface albedos at 0.87  $\mu\text{m}$  wavelength are about two times smaller than their continental counterparts [16]. Small ( $\sim 0.05$ ) and almost season-invariant values of the ocean albedo and the substantial fraction of ocean ( $\sim 0.4$ ) in the retrieved areal-averaged albedos are primarily responsible for the observed “near-flat” seasonal changes of  $A_{0.87}^m$  and  $A_{0.87}^r$  with relatively low peaks ( $\sim 0.25$ ). However, some seasonal changes are evident, and  $A_{0.87}^m$  and  $A_{0.87}^r$  show comparable seasonal

changes over part of our study period. For example,  $A_{0.87}^m$  and  $A_{0.87}^r$  have similar declining trends from the local summer peaks (day of the year (DOY)  $\sim$ 2009.5) to the local fall dips (DOY  $\sim$ 2009.75) and then growing trends to the local winter maximum values (DOY  $\sim$ 2010). However, opposite trends ( $A_{0.87}^m$  versus  $A_{0.87}^r$ ) are observed for other periods (e.g., the end of year 2011). Since the MFRSR-retrieved and MODIS-based areal-averaged albedos at other wavelengths show similar trends (with smaller ranges), we include time series of their albedos at 0.67  $\mu$ m wavelength only (Figure 3). The level of agreement between the MODIS-based and MFRSR-retrieved areal-averaged albedos, on average, gets poorer as the wavelength decreases (from 0.87  $\mu$ m to 0.67  $\mu$ m) (Figure 3). For example,  $A_{0.67}^m$  underestimates  $A_{0.67}^r$  for the 19-month period of interest, and this underestimation can be large (exceeding 100%) during winter. Note that: (1) the sample size of 19 months considered here is quite short for making general statements on the differences between  $A_{\lambda}^m$  and  $A_{\lambda}^r$  during summer and winter, and (2) the relative uncertainties of  $A_{\lambda}^m$  and  $A_{\lambda}^r$  are comparable ( $\sim$ 0.03).

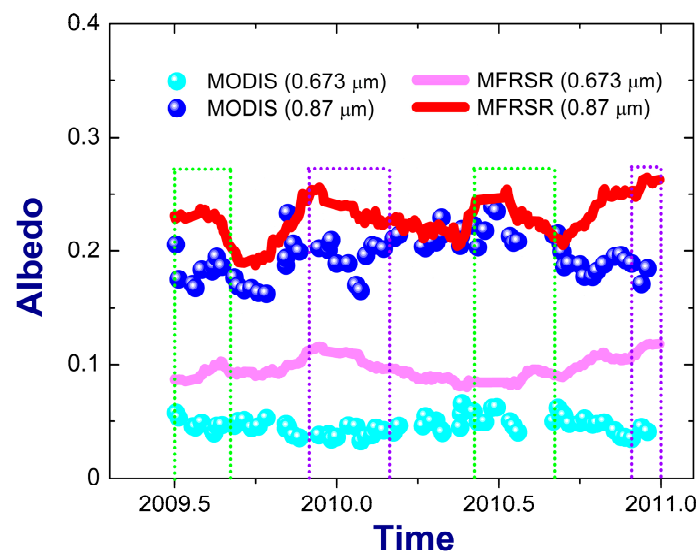


**Figure 3.** Time series of the MFRSR-retrieved areal-averaged surface albedo (red and magenta; boxcar averaging, 16 points) and MODIS-derived albedo for 16-day periods (blue and cyan) at two MFRSR wavelengths (0.673 and 0.87  $\mu$ m) for the 19-month period of interest. Label “time” represents fractional year. Boxes with dotted green and violet lines define summer and winter, respectively.

It is quite interesting that the level of agreement between  $A_{\lambda}^m$  and  $A_{\lambda}^r$  depends on season (winter versus summer). The better agreement, on average, occurs during summer in comparison with winter (Figure 3). The corresponding RMSE values are about 0.04 and 0.06 for summer and winter, respectively (Table 2).

**Table 2.** MODIS-derived and MFRSR-retrieved spectral values of white-sky albedo at four MFRSR wavelengths (0.5, 0.615, 0.673 and 0.87  $\mu$ m). These values are obtained for the 19-month period of interest (“all” columns) and two seasons (“summer” and “winter” columns). The corresponding root mean square error (RMSE) is also included (bottom row).

Wavelength	ALL		SUMMER		WINTER	
( $\mu$ m)	MODIS	MFRSR	MODIS	MFRSR	MODIS	MFRSR
0.5	0.0443	0.0933	0.0465	0.0924	0.0413	0.0993
0.615	0.0488	0.0799	0.0512	0.0869	0.0444	0.0774
0.673	0.0466	0.0959	0.0497	0.0915	0.0396	0.110
0.87	0.196	0.228	0.200	0.234	0.193	0.247
RMSE	0.0411		0.0397		0.0556	

The observed seasonal dependence can be mainly attributed to the two most important factors. The first factor is related to the seasonal changes of wind speed. The mean surface wind speed approximately doubles from about 4 m/s (summer) to about 7 m/s (winter) at the AMF site [36]. The same is true for the maximum seasonal-averaged values of the surface wind speed: about 10 m/s (summer) to above 16 m/s (winter) [14]. The effect of the wind speed increase impacts the albedo in two ways: by expanding coverage of highly-reflective whitecaps [27] and by the increasing fraction of large particles (sea salt) in the atmosphere [36]. These two wind-dependent changes likely represent a challenge for the atmospheric correction process required for determination of the MODIS BRDFs [37]. The second factor is the seasonal change of total cloud fraction. The ARM ground-based observations indicate that the total cloud fraction increases from approximately 60% (summer) to about 80% (winter) at the AMF site [13]. The MODIS BRDF determination requires clear-sky conditions. Since the number of days with clear-sky conditions decreases from summer to winter, the MODIS BRDF determination would be less accurate for winter in comparison with summer. In contrast, the cloudy-sky conditions are favorable for the MFRSR-based retrieval.

For the 19-month period of interest, the MODIS-based albedo noticeably underestimates the MFRSR retrievals and this underestimation depends weakly on the wavelength (Table 2). The corresponding RMSE is 0.04 (Table 2). It should be emphasized that the calculated RMSE represents the highly heterogeneous coastal area (mixture of land and ocean) and it is comparable with that (0.03) obtained for the shortwave areal-averaged albedo over heterogeneous continental areas [5]. The observed negative bias and weak spectral dependence may be governed by several factors, including the estimated fraction of the land/ocean areas and uncertainties of the assumed ocean albedo (Section 3).

Figure 4 illustrates the sensitivity of the calculated RMSE to (1) two assumed parameters of our retrieval, namely the asymmetry factor ( $g$ ) and surface albedo at 0.415  $\mu\text{m}$  wavelength ( $A_{0.415}$ ), and (2) assumed fractions of the ocean areas within box A and circle (Figure 2). Let us start with the impact of  $g$  on the calculated RMSE. The asymmetry factor depends on the droplet effective radius (DER) [38]. There is a wide range (from 5 to 15  $\mu\text{m}$ ) of DER peaks for the 19-month period of interest [13]. However, the corresponding range of  $g$  is quite narrow (from 0.85 to 0.87). We estimate it using a conventional parameterization, which links the DER and  $g$  [38]. It should be mentioned that the MFRSR-retrieved surface albedo ( $A_{\lambda}^r$ ) does not depend on  $g$ , but the retrieved cloud optical depth (COD) does [8]. The small changes of  $g$  (from 0.85 to 0.87) slightly modify the MFRSR-retrieved COD and thus a fraction of “optically thick” cases (COD > 10). The latter are used for calculations of the RMSE. Recall that the “optically thick” cases are favorable for our retrieval of surface albedo [8]. The calculated RMSE depends weakly on the assumed values of  $g$  (Figure 4a): the corresponding RMSE variations are small ( $\sim 0.005$ ). There is a similar weak sensitivity of the calculated RMSE to the substantial ( $\sim 50\%$ ) changes of  $A_{0.415}$  (Figure 4b). The small (0.04) and large (0.06) values of the assumed surface albedo represent roughly  $A_{0.415}$  during summer (wind speed is small) and winter (wind speed is large). Overall, reasonable combined changes of the assumed parameters ( $g$  and  $A_{0.415}$ ) can modify the RMSE only slightly (up to 0.015).

Let us continue with the impact of the assumed fractions of the ocean areas on the calculated RMSE (Figure 4c,d). The increase of ocean fraction within box A (Figure 2) increases the corresponding land surface albedo ( $A_{\lambda,land}^A$ ) and thus the MODIS-based areal-averaged surface albedo ( $A_{\lambda}^m$ ). Doubling this fraction (from 0.1 to 0.2) reduces the RMSE slightly ( $\sim 0.007$ ) (Figure 4c). This reduction likely defines the upper limit of the expected range. The ocean fraction within the circle (Figure 2) gets larger with the increase of the circle area associated with larger CBH [8]. Seasonal changes of CBH averages are substantial for the 19-month period of interest [13]. For example, these averages are 0.76 km and 1.14 km for the summer and winter, respectively [13]. The corresponding standard deviations are large and comparable: 0.48 km (winter) and 0.47 km (summer) [13]. To account for the large seasonal variations of CBH and thus of the CBH-dependent circle area, we calculate the RMSE using a substantial range (from 0.3 to 0.5) of the assumed ocean fraction within the circle (Figure 4d). The small (0.3) and

large (0.5) values of the assumed ocean fractions represent roughly the 5th (CBH ~0.3 km) summer percentile and 95th (CBH ~1.6 km) winter percentile of CBH [13]. The substantial (~67%) increase of the ocean fraction within the circle area increases the RMSE slightly (~0.02) (Figure 4d). Overall, the near-extreme combined changes of the assumed ocean fractions (within box A and the circle) can modify the RMSE slightly (up to 0.03).

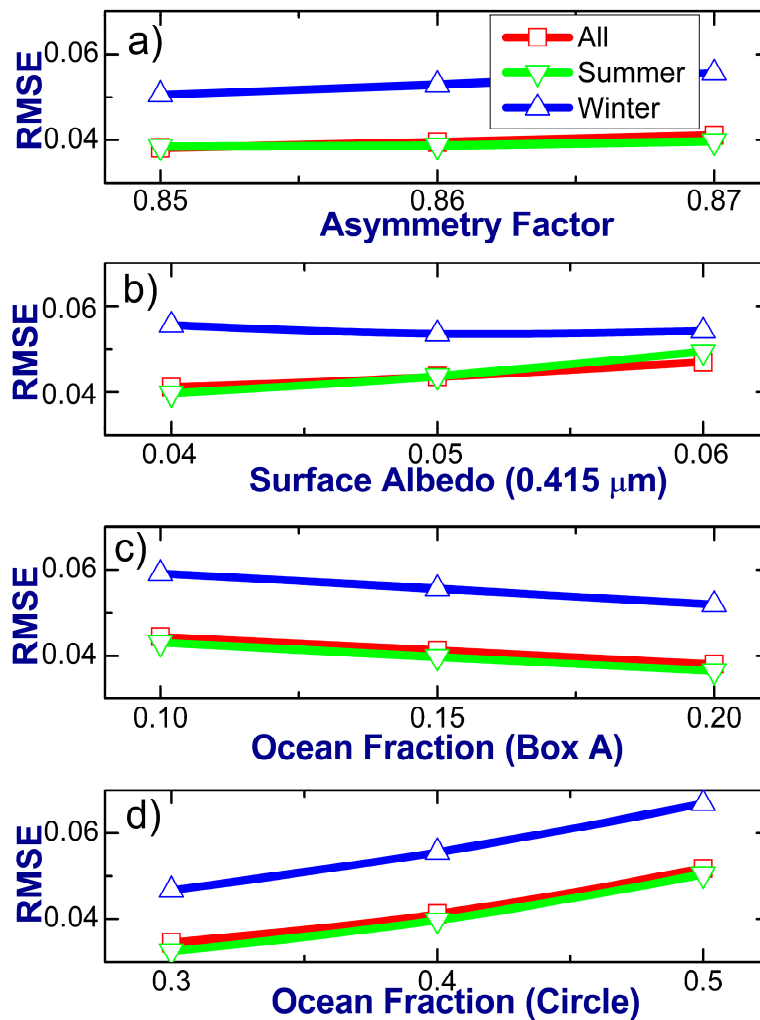


**Figure 4.** The calculated RMSE as a function of the assumed asymmetry factor (a), surface albedo at 0.415 μm wavelength (b), fractions of the ocean areas within box A (c), and circle (d). The calculated RMSE for the 19-month period of interest (All) and two seasons (Summer and Winter) are indicated by red, green and blue colors, respectively.

Figure 5 demonstrates that a reasonable agreement between the composite-based albedo and the other two areal-averaged albedos is achievable within the given level of uncertainty. Moreover, the composite-based albedo properly captures the spectral changes of the areal-averaged albedos and shows a pronounced dip around 0.66 μm wavelength similar to  $A_{\lambda}^r$  and  $A_{\lambda}^m$  (Figure 5).

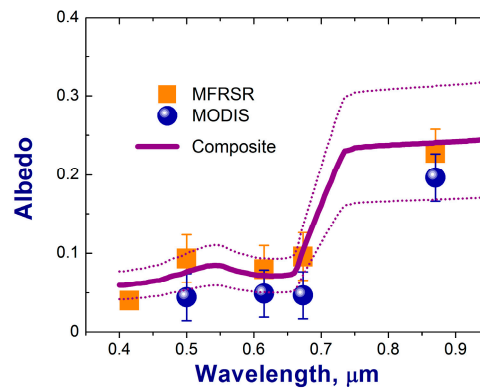


**Figure 5.** Spectral values for the MFRSR-retrieved (orange squares), MODIS-derived (blue dots) and composite-based (solid violet line) areal-averaged albedos. The MFRSR-retrieved and MODIS-derived mean values are obtained for the 19-month period of interest; their error bars represent the corresponding uncertainties. The uncertainty of the composite method is shown by the dotted violet lines.

## 5. Summary

In this study, we assess the performance of our retrieval of areal-averaged surface albedo [8] under challenging coastal conditions, where there exist distinct and abrupt differences in local surface albedo (land versus ocean). We use an integrated dataset collected during a 19-month (June 2009–December 2010) period at the ARM Mobile Facility (AMF) site located on the northern coast of Graciosa Island, Azores [12]. This dataset includes the atmospheric transmission measured by a ground-based Multi-Filter Rotating Shadowband Radiometer (MFRSR) at five wavelengths (0.415, 0.5, 0.615, 0.673 and 0.87  $\mu\text{m}$ ). We apply the MFRSR-measured transmission to retrieve the spectrally resolved areal-averaged surface albedo and compare it with those obtained from collocated and coincident MODIS data and composite-based estimates. For our comparison, we utilize the MODIS-derived white-sky surface albedos. To facilitate this comparison, these albedos are extrapolated/interpolated from the four nominal MODIS wavelengths (0.47, 0.56, 0.67 and 0.86  $\mu\text{m}$ ) to the four MFRSR wavelengths (0.5, 0.615, 0.673 and 0.87  $\mu\text{m}$ ). We show that the corresponding root mean square error (RMSE), which is defined as the root mean squared difference between the MODIS surface albedo and the retrieved surface albedo (0.04) is comparable with that (0.03) obtained previously for the shortwave areal-averaged albedo over heterogeneous continental areas [5].

We also demonstrate that, on average, the MODIS areal-averaged albedo underestimates the MFRSR-retrieved albedo and this underestimation (0.03–0.04) depends weakly on wavelength. Similar underestimation (0.025–0.05) was obtained earlier over heterogeneous continental areas when the spectral areal-averaged albedos estimated from different platforms—MODIS data versus aircraft measurements—were compared [34]. We calculate a composite-based albedo for multiple wavelengths within the spectral range of interest (0.4–0.9  $\mu\text{m}$ ) using a weighted-average approach, which requires one to define fractions of major surface types estimated in an area ( $\sim 2 \times 2 \text{ km}^2$ ) surrounding this coastal site and albedo for these surface types. The surface albedo obtained by three methods considered here (MFRSR measurements, MODIS data and composite-based outputs) with comparable relative uncertainty ( $\sim 0.03$ ) exhibit similar spectral signatures with a marked drop in the surface albedo around 0.66  $\mu\text{m}$  wavelength. Depending on the choice made (i.e., between MFRSR or MODIS), good agreement between the composite-based and MFRSR/MODIS areal-averaged albedos is possible, and thus any of these three methods would be a good choice for determining the albedo—although the MFRSR/MODIS methods may be easier to apply.

Measurements of atmospheric transmission are relatively ubiquitous and inexpensive compared to tower-based observations of the spectrally-resolved surface albedo. The existing transmission data, for instance, can be obtained at many permanent [9,10] and temporary (e.g., ARM Mobile

Facilities; [39]) sites worldwide with various degrees of surface heterogeneity. The transmission-based approach used in this study offers the opportunity to monitor the multi-spectral surface albedo at climatically important regions and is a valuable complementary tool to the conventional satellite- and tower-based methods. The anticipated information on the multi-spectral areal-averaged surface albedo provided by transmission-based approach together with other related data would be beneficial for validation and improvement of existing and future parameterizations of the surface albedo in atmospheric models.

**Acknowledgments:** This work is supported by the Office of Biological and Environmental Research (OBER) of the US Department of Energy (DOE) as part of the Atmospheric Radiation Measurement (ARM) and Atmospheric System Research (ASR) programs. The Pacific Northwest National Laboratory (PNNL) is operated by Battelle for the DOE under contract DE-A06-76RLO 1830. The MODIS MCD43C2 v5 surface albedo BRDF data were acquired from the Land Processes (LP) Distributed Active Archive Center (DAAC), (<https://lpdaac.usgs.gov/>).

**Author Contributions:** Abstract (E. Kassianov, J. Barnard), Introduction (E. Kassianov, J. Barnard), Approach (all), Results (all), Summary (all). E. Kassianov led the research and manuscript preparation. J. Barnard supervised research and manuscript writing. All authors contributed to data analysis. We are grateful to four anonymous reviewers for thoughtful comments.

**Conflicts of Interest:** The authors declare no conflict of interest.

## References

1. Myhre, G.; Myhre, A. Uncertainties in radiative forcing due to surface albedo changes caused by land-use changes. *Climate* **2003**, *16*, 1511–1524. [[CrossRef](#)]
2. Ghimire, B.; Williams, C.A.; Masek, J.; Gao, F.; Wang, Z.; Schaaf, C.; He, T. Global albedo change and radiative cooling from anthropogenic land cover change, 1700 to 2005 based on MODIS, land use harmonization, radiative kernels, and reanalysis. *Geophys. Res. Lett.* **2014**, *41*, 9087–9096. [[CrossRef](#)]
3. Wendisch, M.; Pilewskie, P.; Jäkel, E.; Schmidt, S.; Pommier, J.; Howard, S.; Jonsson, H.H.; Guan, H.; Schröder, M.; Mayer, B. Airborne measurements of areal spectral surface albedo over different sea and land surfaces. *J. Geophys. Res.* **2004**, *109*, D08203. [[CrossRef](#)]
4. Liang, S.; Fang, H.; Chen, M.; Shuey, C.; Walthall, C.; Doughtry, C.; Morisette, J.; Schaaf, C.; Strahler, A. Validating MODIS land surface reflectance and albedo products: Methods and preliminary results. *Remote Sens. Environ.* **2002**, *83*, 149–162. [[CrossRef](#)]
5. Wang, Z.; Schaaf, C.; Strahler, A.H.; Chopping, M.J.; Román, M.O.; Shuai, Y.; Woodcock, C.E.; Hollingerg, D.Y.; Fitzjarrald, D.R. Evaluation of MODIS albedo product (MCD43A) over grassland, agriculture and forest surface types during dormant and snow-covered periods. *Remote Sens. Environ.* **2014**, *140*, 60–77. [[CrossRef](#)]
6. Wang, K.; Liang, S.; Schaaf, C.L.; Strahler, A.H. Evaluation of Moderate Resolution Imaging Spectroradiometer land surface visible and shortwave albedo products at FLUXNET sites. *J. Geophys. Res.* **2010**, *115*, D17107. [[CrossRef](#)]
7. Cescatti, A.; Marcolla, B.; Vannan, S.K.S.; Pan, J.Y.; Román, M.O.; Yang, X.; Ciaia, P.; Cook, R.B.; Law, B.E.; Matteucci, G.; et al. Intercomparison of MODIS albedo retrievals and in situ measurements across the global FLUXNET network. *Remote Sens. Environ.* **2012**, *121*, 323–334. [[CrossRef](#)]
8. Kassianov, E.; Barnard, J.; Flynn, C.; Riihimäki, L.; Michalsky, J.; Hodges, G. Areal-averaged spectral surface albedo from ground-based transmission data alone: Toward an operational retrieval. *Atmosphere* **2014**, *5*, 597–621. [[CrossRef](#)]
9. Augustine, J.A.; Cornwall, C.R.; Hodges, G.B.; Long, C.N.; Medina, C.I.; DeLuisi, J.J. An automated method of MFRSR calibration for aerosol optical depth analysis with application to an Asian dust outbreak over the United States. *J. Appl. Meteor.* **2003**, *42*, 266–278. [[CrossRef](#)]
10. Michalsky, J.; Hodges, G.; Field, B. Measured spectral albedo—Four years of data from the Western U.S. Prairie. *Geophys. Res. Atmos.* **2013**, *118*, 813–825. [[CrossRef](#)]
11. Miller, M.A.; Nitschke, K.; Ackerman, T.P.; Ferrell, W.R.; Hickmon, N.; Ivey, M. The ARM Mobile Facilities. In *The Atmospheric Radiation Measurement (ARM) Program: The First 20 Years*; Meteorological Monographs; American Meteorological Society: Boston, MA, USA, 2016. [[CrossRef](#)]
12. The AMF deployment. Available online: <https://www.arm.gov/research/campaigns/amf2009clapmb1> (accessed on 30 June 2017).

13. Dong, X.; Xi, B.; Kennedy, A.; Minnis, P.; Wood, R. A 19-month record of marine aerosol–cloud–radiation properties derived from DOE ARM Mobile Facility Deployment at the Azores. Part I: Cloud fraction and single-layered MBL cloud properties. *Climate* **2014**, *27*, 3665–3682. [CrossRef]
14. Wood, R.; Wyant, M.; Bretherton, C.S.; Rémillard, J.; Kollias, P.; Fletcher, J.; Stemmler, J.; de Szoeko, S.; Yuter, S.; Miller, M.; et al. Clouds, aerosols, and precipitation in the marine boundary layer: An ARM Mobile Facility deployment. *Bull. Am. Meteor. Soc.* **2015**, *96*, 419–440. [CrossRef]
15. Jin, Z.; Charlock, T.P.; Smith, W.L., Jr.; Rutledge, K. A parameterization of ocean surface albedo. *Geophys. Res. Lett.* **2004**, *31*, L22301. [CrossRef]
16. McFarlane, S.; Gaustad, K.; Mlawer, E.; Long, C.; Delamere, J. Development of a high spectral resolution surface albedo product for the ARM Southern Great Plains central facility. *Atmos. Meas. Tech.* **2011**, *4*, 1713–1733. [CrossRef]
17. Varotsos, C.A.; Melnikova, I.N.; Cracknell, A.P.; Tzanis, C.; Vasilyev, A.V. New spectral functions of the near-ground albedo derived from aircraft diffraction spectrometer observations. *Atmos. Chem. Phys.* **2014**, *14*, 6953–6965. [CrossRef]
18. Eastern North Atlantic (ENA). Available online: <https://www.flickr.com/photos/armgov/sets/72157629622837705> (accessed on 30 June 2017).
19. Sun, L.; Schulz, K. The improvement of land cover classification by thermal remote sensing. *Remote Sens.* **2015**, *7*, 8368–8390. [CrossRef]
20. Oleson, K.W.; Lawrence, D.M.; Bonan, G.B.; Drewniak, B.; Huang, M.; Koven, C.D.; Levis, S.; Li, F.; Riley, W.J.; Subin, Z.M.; et al. *Technical description of version 4.5 of the Community Land Model (CLM)*; NACR/TN-487+STR/NACR Technical Note; National Center for Atmospheric Research: Boulder, CO, USA, 2013; p. 420.
21. Gao, F.; He, T.; Wang, Z.; Ghimire, B.; Shuai, Y.; Masek, J.; Schaaf, C.; Williams, C. Multiscale climatological albedo look-up maps derived from moderate resolution imaging spectroradiometer BRDF/albedo products. *Appl. Remote Sens.* **2014**, *8*, 15. [CrossRef]
22. Rowe, C.M. Incorporating landscape heterogeneity in land surface albedo models. *Geophys. Res.* **1993**, *98*, 5037–5043. [CrossRef]
23. Ricchiazzi, P.; Yang, S.; Gautier, C.; Soble, D. SBDART: A research and Teaching software tool for plane-parallel radiative transfer in the Earth’s atmosphere. *Bull. Am. Meteor. Soc.* **1998**, *79*, 2101–2114. [CrossRef]
24. ASTER Spectral Library. Available online: <http://speclib.jpl.nasa.gov/> (accessed on 30 June 2017).
25. Barnes, B.B.; Hu, C.; Schaeffer, B.A.; Lee, Z.; Palandro, D.A.; Lehrter, J.C. MODIS-derived spatiotemporal water clarity patterns in optically shallow Florida Keys waters: A new approach to remove bottom contamination. *Remote Sens. Environ.* **2013**, *134*, 377–391. [CrossRef]
26. Liu, S.; Roujean, J.L.; Kaptué Tchuenté, A.; Calvet, J.C.; Ceamanos, X. A parameterization of SEVIRI and MODIS daily surface albedo with soil moisture: Calibration and validation over southwestern France. *Remote Sens. Environ.* **2014**, *144*, 137–151. [CrossRef]
27. Schwendeman, M.; Thomson, J. Observations of whitecap coverage and the relation to wind stress, wave slope, and turbulent dissipation. *Geophys. Res. Oceans.* **2015**, *120*, 8346–8363. [CrossRef]
28. Whitlock, C.H.; Bartlett, D.S.; Gurganus, E.A. Sea foam reflectance and influence on optimum wavelength for remote sensing of ocean aerosols. *Geophys. Res. Lett.* **1982**, *9*, 719–722. [CrossRef]
29. The MODIS Product MCD43C2 v005. Available online: [https://lpdaac.usgs.gov/dataset\\_discovery/modis/modis\\_products\\_table/mcd43c2](https://lpdaac.usgs.gov/dataset_discovery/modis/modis_products_table/mcd43c2) (accessed on 30 June 2017).
30. Gao, F.; Schaff, C.B.; Strahler, A.H.; Roesch, A.; Lucht, W.; Dickinson, R. MODIS bi-directional reflectance distribution function and albedo Climate Modeling Grid products and the variability of albedo for major global vegetation types. *Geophys. Res.* **2005**, *110*, D01104. [CrossRef]
31. Schaaf, C.B.; Gao, F.; Strahler, A.H.; Lucht, W.; Li, X.; Tsang, T.; Strugnell, N.C.; Zhang, X.; Jin, Y.; Muller, J.P.; et al. First operational BRDF albedo nadir reflectance products from MODIS. *Remote Sens. Environ.* **2002**, *83*, 135–148. [CrossRef]
32. Liang, S.; Strahler, A.H.; Walthall, C.W. Retrieval of land surface albedo from satellite observations: A simulation study. *Appl. Meteorol.* **1999**, *38*, 712–725. [CrossRef]

33. Salomon, J.G.; Strahler, A.H.; Gao, F.; Jin, Y. Validation of the MODIS bi-directional reflectance distribution function and albedo retrievals using combined observation from the Aqua and Terra platforms. *IEEE Trans. Geosci. Remote Sens.* **2006**, *44*, 1555–1564. [[CrossRef](#)]
34. Coddington, O.; Schmidt, K.S.; Pilewskie, P.; Gore, W.J.; Bergstrom, R.W.; Román, M.; Redemann, J.; Russell, P.B.; Liu, J.; Schaaf, C.C. Aircraft measurements of spectral surface albedo and its consistency with ground-based and space-borne observations. *Geophys. Res.* **2008**, *113*, D17209. [[CrossRef](#)]
35. MODIS albedo product (MCD43A). Available online: [https://www.umb.edu/spectralmass/terra\\_aqua\\_modis/modis\\_brd\\_f\\_albedo\\_product\\_mcd43](https://www.umb.edu/spectralmass/terra_aqua_modis/modis_brd_f_albedo_product_mcd43) (accessed on 30 June 2017).
36. Logan, T.; Xi, B.; Dong, X. Aerosol properties and their influences on marine boundary layer cloud condensation nuclei at the ARM mobile facility over the Azores. *Geophys. Res. Atmos.* **2014**, *119*, 4859–4872. [[CrossRef](#)]
37. Vermote, E.; Kotchenova, S. MODIS directional surface reflectance product: Method, error estimates and validation. In *Land Remote Sensing and Global Environmental Change: NASA's Earth Observing System and the Science of ASTER and MODIS*; Ramachandran, B., Justice, C.O., Abrams, M.J., Eds.; Springer: New York, NY, USA, 2011; pp. 533–547.
38. Hu, Y.X.; Stamnes, K. An accurate parameterization of the radiative properties of water clouds suitable for use in climate models. *J. Clim.* **1993**, *6*, 728–742. [[CrossRef](#)]
39. ARM Mobile Facilities. Available online: <http://www.arm.gov/sites/amf> (accessed on 30 June 2017).



© 2017 by the authors. Licensee MDPI, Basel, Switzerland. This article is an open access article distributed under the terms and conditions of the Creative Commons Attribution (CC BY) license (<http://creativecommons.org/licenses/by/4.0/>).